Eurographics Symposium on Geometry Processing 2018
T. Ju and A. Vaxman
(Guest Editors)

Volume 37 (2018), Number 5

A unified discrete framework for intrinsic and extrinsic Dirac operators for geometry processing

Zi Ye[1], Olga Diamanti[2,3], Chengcheng Tang[2], Leonidas Guibas[2], Tim Hoffmann[1]

[1] Technical University of Munich [2] Stanford University [3] Autodesk Research

Abstract

Spectral mesh analysis and processing methods, namely ones that utilize eigenvalues and eigenfunctions of linear operators on meshes, have been applied to numerous geometric processing applications. The operator used predominantly in these methods is the Laplace-Beltrami operator, which has the often-cited property that it is intrinsic, namely invariant to isometric deformation of the underlying geometry, including rigid transformations. Depending on the application, this can be either an advantage or a drawback. Recent work has proposed the alternative of using the Dirac operator on surfaces for spectral processing. The available versions of the Dirac operator either only focus on the extrinsic version, or introduce a range of mixed operators on a spectrum between fully extrinsic Dirac operator and intrinsic Laplace operator. In this work, we introduce a unified discretization scheme that describes both an extrinsic and intrinsic Dirac operator on meshes, based on their continuous counterparts on smooth manifolds. In this discretization, both operators are very closely related, and preserve their key properties from the smooth case. We showcase various applications of our operators, with improved numerics over prior work.

Categories and Subject Descriptors (according to ACM CCS): I.3.5 [Computer Graphics]: Computational Geometry and Object Modeling—Geometric algorithms, languages, and systems

1. Introduction

Many applications in geometric analysis and processing have benefited from *spectral* methods, namely ones that utilize eigenvalues and eigenfunctions of linear operators defined on the underlying geometric object – typically a polygonal mesh. Applications include mesh segmentation, feature extraction, mappings and correspondence, smoothing, deformation, remeshing, and various others [LZ10]. Various properties of spectral methods have made them popular in geometry processing: the frequency domain, namely the space spanned by the operator eigenfunctions, typically enables multi-resolution shape analysis via independent processing of the various "frequencies", and allows for a level of mesh independence. It also provides a canonical space on which to map shapes so as to jointly perform operations on multiple shapes simultaneously.

Among the operators used for spectral analysis, the Laplace-Beltrami operator is the most ubiquitous. The Laplace-Beltrami operator acts on the space of scalar functions defined on the shape, is elliptic and self-adjoint, and thus its eigenfunctions provide a basis on which it is possible to express any real-valued signal defined on the mesh. One of the appealing properties of the Laplacian operator is that it is *intrinsic*, namely it is invariant to isometric deformation of the underlying geometry, including rigid transformations. Hence, any analysis, filtering, or processing done using its eigenfunctions will similarly be independent of such transformations.

However, recent works in geometry processing [LJC17, CSBC*17] have pointed out that often, capturing extrinsic information can be useful for some applications; for example, in order to distinguish between dissimilar shapes that are however intrinsically similar, e.g. a cylinder and a plane, or different poses of the same shape. To address this issue, Liu et al. [LJC17] propose to use operators inspired by the quaternionic *Dirac operator*, which acts on the space of *quaternions* defined on a mesh. The extrinsic version of the Dirac operator was introduced in the geometry processing literature in the context of conformal deformations by Crane et al. [CPS11]. Liu et al. introduced a parameterizable family of operators obtained by interpolating between a fully intrinsic and a fully extrinsic operator via a user-defined parameter. These two operators correspond to the fully intrinsic and the fully extrinsic part extracted from the square of the extrinsic Dirac operator of [CPS11]; the fully intrinsic operator is in fact a quaternionic Laplacian operator on the mesh. By interpolating, Liu et al. enable a trade-off between the intrinsic vs. extrinsic nature of these two operators. The classical Dirac operator has a well-known relation to pointwise conformal transformations that are *integrable*, namely map closed surfaces to closed surfaces. This property has also been exploited in the discrete case [Cra13] to design conformal deformations on meshes. This property no longer holds for the square of the Dirac operator in [LJC17].

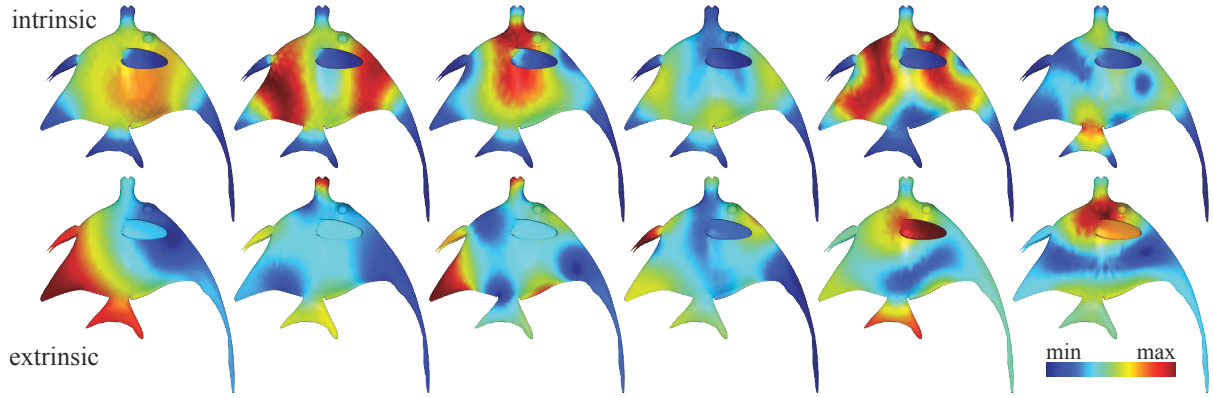

Figure 1: *The eigenfunction magnitudes of the intrinsic and extrinsic Dirac operators, discretized in a unified way using our framework. The two operators capture different geometric information on meshes, highlighting different types of distortion and bending / stretching. Intrinsic Dirac eigenfunctions attain low values in regions of high Gaussian curvature – extrinsic eigenfunctions manifest maxima in curvy regions.*

In this paper, we introduce a unified discretization that can describe not only the extrinsic Dirac operator, but also an intrinsic version of it, on polygonal meshes, based on the continuous Dirac operator definitions. In this discretization, both operators are very closely related, and remain compatible with their smooth counterparts, thus preserving their key properties. Using the extrinsic operator, we can still define and apply conformal transformations as originally done in Crane et al. [CPS11]. On the other hand, the intrinsic operator can be directly used in applications where invariance to isometries is necessary, e.g. feature extraction or segmentation. The intrinsic operator can also be used to extract the "spinor harmonics" of an arbitrary discrete surface. While this was shown previously for the particular case of spheres using the *extrinsic* operator of [CPS11], the canonical shapes derived as spinor harmonics from an extrinsic operator tend to exaggerate the regions with high curvature on general surfaces. Instead, the spinor harmonics obtained using our new *intrinsic* Dirac operator look much more reasonable and are invariant under edge-length-preserving deformations. We analyze various properties of our operator to gain insight into its accuracy, and showcase frequently improved numerics over previous operators. By studying its eigenfunctions and eigenvalues, we provide initial theoretical results on properties pertaining to the eigenfunctions that remain invariant under rigid or general isometric transformations. These considerations are useful when using the operator for applications. In this paper, we apply our operator for curvature painting (Fig. 7), canonical shape construction (Fig. 10 and 9), fast surface fairing (Fig. 15), shape correspondence (Fig. 12) and close-to-conformal shape filtering (Fig. 16). As future work, further applications can be considered, among which feature extraction, object classification, shape correspondence, deformation transfer and distance calculations. We hope that the availability of an intrinsic and extrinsic quaternionic operator discretized within the same framework will inspire further such applications using spectral methods.

2. Related Work

Spectral Mesh Processing. Frequency-based ideas have been widely used for mesh analysis and processing in a broad range of applications - see [LZ10] and papers therein for a recent survey. The majority of these works utilize the spectrum (eigenfunctions / eigenvalues) of the Laplace-Beltrami operator on discrete manifolds [DRW10] – mostly triangular meshes, although extensions to polygonal cases exist [HKA15]. Applications include, among others, mesh smoothing, compression, shape segmentation, matching, and parameterization. More recently, the spectral approach was also involved in on-surface distance approximation [LRF10], feature extraction [SOG09, Rus10, ASC11], mesh editing [HSTP11], remeshing [LHJ*14], inter-surface functional-based mappings [OBCS*12] and on-surface tangent field design and processing [ABCCO13, ACBCO17, AOCBC15]. The Laplace-Beltrami operator acts on functions defined on a manifold. Instead, our work uses a discrete version of the *Dirac operator*, acting on quaternionic functions on manifolds. In the continuous case, the square of the Dirac operator closely relates to the Laplace-Beltrami.

Continuous Dirac Operators. In the continuous setting, an *extrinsic* version of the Dirac operator D_f, namely one that depends on the three-dimensional immersion of a surface, was defined by Kamberov et al. [KPP98, Kam02]. An *intrinsic* Dirac operator D, depending only on the Riemannian metric and algebraic structure of the manifold and not on embedding coordinates, has been known in the mathematical community since Atiyah and Singer [AS63]. In particular, for an immersed surface in $\mathbb{R}^3$, these two operators D_f and D are related by a simple formula $D_f = D - H$, where H is the mean curvature of the surface seen as as diagonal operator.

The spectrum of the intrinsic Dirac operator has also been studied [Gin09]. The Dirac operator is the most fundamental elliptic operator on manifolds [Esp98, section 3.6], indicating that Dirac spectra are supposed to contain more information than the Laplacian spectra (for evidence see Fig. 5). More importantly, the Dirac operator can be used to design conformal deformations of an input surface, by prescribing the desired change in mean curvature half density [KPP98] and solving an eigenvalue-like condition.

Discrete Dirac Operators. The Dirac operator closest to ours is the discrete extrinsic operator introduced by Crane et al. [CPS11],

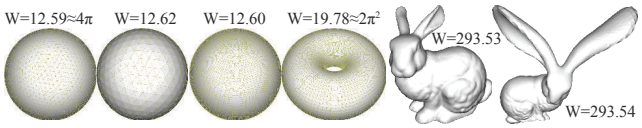

Figure 2: *On the left, comparing our discrete Willmore energy to its known values for the sphere and torus (left). On the right, comparing the energy values for two surfaces, one of which is a Möbius transformation of the other.*

with applications such as curvature painting for conformal deformations and conformal surface fairing [CPS13]. More recently, Liu et al. [LJC17] noticed that the operator obtained by squaring Crane et al.'s Dirac operator can be decomposed into a purely intrinsic and a purely extrinsic part. They then introduced a family of operators covering the spectrum between these two ends, and showcased the usefulness of the extrinsicness vs. intrinsicness of their operators for various applications. [KJP*18] utilize this Dirac operator to build a generative neural network for 3D shapes.

Several other notable Dirac operators exist, though less related to ours. [LS16] defines a discrete Hodge-Dirac operator in the framework of finite element exterior calculus. This operator is defined on the cotangent bundle and its exterior algebra; instead, our operator is defined on the spinor bundle. It remains an interesting question whether the discretization of [LS16] can be applied on the surface conformal transformation problem; additionally, their thorough analysis of stability and convergence could inspire future work on our operator. [LP18] describes an exact Dirac operator, corresponding to infinitesimal conformal transformations.

3. Preliminaries

In this section we expose some of the notions pertaining to the Dirac operator as known in the continuous case that will become relevant at later sections of the paper.

3.1. Quaternions

Our Dirac operators operate on *spinors* on manifold surfaces; in the case where an explicit three-dimensional immersion of the surface exists, spinors can be roughly understood as fields of *quaternions* defined on the surface. The space $\mathbb{H}$ of quaternions consists of the 4-dimensional vectors $q = a + bi + cj + dk$ expressed as a linear combination of the basis $\{1, i, j, k\}$ endowed with the multiplicative structure $i^2 = j^2 = k^2 = -1$, $i \cdot j = -j \cdot i = k$, $j \cdot k = -k \cdot j = i$, $k \cdot i = -i \cdot k = j$. The norm of the quaternion is given by $|q| = \sqrt{a^2 + b^2 + c^2 + d^2}$.

Throughout this paper we frequently identify the ambient 3D space $\mathbb{R}^3$ with the subspace of $\mathbb{H}$ containing only the purely imaginary quaternions $\mathrm{Im}(\mathbb{H})$, via the mapping $(x, y, z) \mapsto xi + yj + zk$. Unit norm quaternions can be used to represent arbitrary rotations in $\mathbb{R}^3$: a rotation around an axis v by an angle θ can be expressed using the unit-norm quaternion $q = \pm(\cos\frac{\theta}{2} - \sin\frac{\theta}{2}v)$. The rotated position of a point $u \in \mathbb{R}^3$ will then be given by $u \mapsto q^{-1} \cdot u \cdot q$. Quaternions of norm different than 1 can represent combinations of rotations with scaling (namely, similarity transformations), where the scaling factor is given by $|q|^2$. The transformed point will then be given by $u \mapsto \overline{q} \cdot u \cdot q$.

Under the identification of $\mathbb{R}^3$ with $\mathrm{Im}(\mathbb{H})$, a 3D surface can be thought of as a map from an abstract surface onto 3D space $f : M \to \mathbb{H}$ [CPS11]. The differential of the mapping $df : TM \mapsto \mathbb{H}$ maps between vectors $\mathbf{x}$ in the tangent space of M and vectors in 3D space. If a 2D parameterization of the manifold surface is available, this would be the standard pointwise 2×3 Jacobian matrix. In this paper we are interested in immersed surfaces, namely such that the map df does not degenerate.

3.2. The extrinsic Dirac operator and the spin transformation

An extrinsic Dirac operator was proposed by Kamberov et al. in [KPP98] and its discrete version in [CPS11]. Let $f : M \to \mathbb{H}$ be an immersed simply-connected surface in $\mathbb{R}^3$. Assume we deform the surface by rotating and scaling each tangent plane locally but in a smooth way. This process can be expressed as a pointwise quaternionic transformation on the tangent planes, namely changing the map df by $\tilde{df} = \overline{\phi} \cdot df \cdot \phi$, where $\phi \in \Omega(\mathbb{H}) := M \to \mathbb{H}$ is a smooth quaternion-valued function. In general, such a per-element transformation will not be *integrable*: it will not be generally possible to "stitch up" these new planes $\tilde{df}$ to create a surface such that these planes will be tangent to it. For $\tilde{df}$ to indeed be the differential of any surface, it must satisfy $d\tilde{df} = 0$, which [CPS11] is equivalent to the Dirac equation

$$D_f \phi = \rho \phi \tag{1}$$

where $\rho : M \to \mathbb{R}$ is some real-valued function, and

$$D_f \phi := -\frac{df \wedge d\phi}{|df|^2} \tag{2}$$

defines the *extrinsic* Dirac operator D_f on the space of smooth quaternionic-valued functions ; division by the volume form $|df|^2$ corresponds to the Hodge dual. Transformations that satisfy (1) are called *spin transformations* and correspond to conformal deformations of the surface; the function ρ controls the deformation locally. Note that plain eigenfunctions of the self-adjoint Dirac operator D_f correspond to ρ being constant-valued on the surface, with the constant value determined by the corresponding eigenvalue. Thus, such eigenfunctions also induce conformal immersions.

The geometric meaning of the ρ function relates to the change in curvature induced by the transformation. More specifically, let us define the *length element* $|df|$ of the surface by $|df(\mathbf{x})|^2 = g(\mathbf{x}, \mathbf{x})$ where $g(\mathbf{x}, \mathbf{y}) = \langle df(\mathbf{x}), df(\mathbf{y}) \rangle, \mathbf{x}, \mathbf{y} \in TM$ the surface metric. The *mean curvature half density* of the surface is defined by $h := H|df|$ where H the mean curvature of the surface. Then [KPP98], ρ measures the change of this quantity as the surface is transformed

$$\tilde{h} = \tilde{H}|\tilde{df}| = h + \rho|df| \tag{3}$$

and the mean curvature of the new surface is $\tilde{H} = (\rho + H)/|\phi|^2$. One can thus design and manipulate a scalar function ρ to conformally deform a surface to match a target mean curvature half density. If M is not simply-connected, then the Dirac equation (1) actually gives an immersion of its universal covering $\tilde{M} \to \mathbb{R}^3$ instead, namely, the transformed surface may not "close up" globally [CPS11].

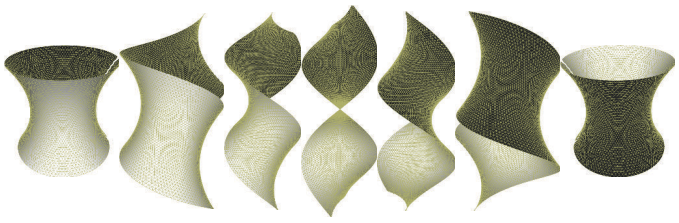

Figure 3: *A family of discrete minimal surfaces.*

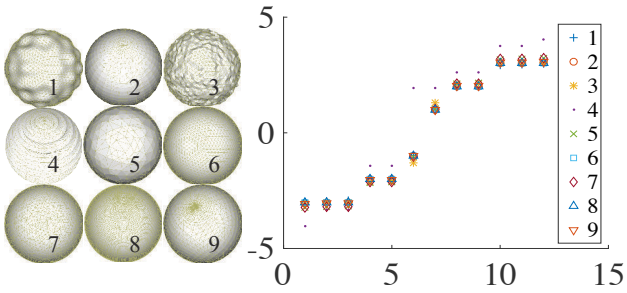

Figure 4: *The eigenvalues of our discrete intrinsic Dirac operator, computed on various meshings of spheres, agree with their known values from the continuous case. The only exception is the fourth mesh with really bad normal approximation. Additionally, they are relatively robust against noise in the meshing or the geometry.*

3.3. The intrinsic Dirac operator

For an abstract, non-immersed oriented surface M, with Riemannian metric (and some additional *spin* structure) an intrinsic Dirac operator has been defined that depends only on the surface metric [LM16]. For a fully rigorous definition of this operator, the notion of spinors and spin manifold structures needs to be introduced, which is beyond the scope of this paper – a good introduction can be found in [Cno02]. The spinor bundle $\mathcal{S} \to M$ is a vector bundle, whose fibers $\mathcal{S}_x$ at each point x are isomorphic to the quaternions, and its transition functions are, in some sense, the square root of the transition functions of the tangent bundle $TM \to M$. Hence, the sections of the spinor bundle $\Omega(\mathcal{S})$, called the spinor fields, are locally quaternion-valued functions. The intrinsic Dirac operator $D : \Omega(\mathcal{S}) \to \Omega(\mathcal{S})$ is a first-order differential operator defined by

$$D\phi = e_1 \cdot \nabla_{e_1}\phi + e_2 \cdot \nabla_{e_2}\phi, \tag{4}$$

where ∇ is the connection on the spinor bundle, induced by the Levi-Civita connection and the multiplication is called the Clifford multiplication which can be understood locally as the quaternion multiplication. For the purposes of this papar, we always assume that the surface is endowed with an immersion $f : M \to \mathbb{R}^3$. Then, the spinor bundle can be identified with the ambient trivial spinor bundle and therefore, the spinor fields would simply reduce to the quaternion-valued functions on the surface. As a result, the intrinsic Dirac operator can be equivalently defined by

$$D = D_f + H \tag{5}$$

where H the mean curvature of the surface. From this formula it is not trivial to see that D is intrinsic. We prove the intrinsicness of our discrete setting in the appendix (Proof of Theorem 4.3). In the general smooth case, it can be shown that (4) and (5) only differ by a gauge transformation [Chu16]. Combining (5) with (1) and (3), it is easy to see that any smooth spinor field $\phi \in \Omega(\mathcal{S})$ satisfying

$$D\phi = \rho\phi, \tag{6}$$

where ρ is real-valued scalar function, gives a conformal immersion $M \to \mathbb{R}^3$ with the mean curvature half-density

$$\tilde{h} = \tilde{H}|d\tilde{f}| = \rho|df| \tag{7}$$

and the mean curvature $\tilde{H} = \rho/|\phi|^2$ [Fri98].

4. Method

We have so far described the intrinsic and extrinsic Dirac operators in the continuous case. We will now propose our discretizations of the operators on polygonal meshes, which preserve some of their continuous properties; most importantly, the relation to integrable conformal spin transformations of surfaces (Eq.(1), (6)).

4.1. Discretization

Face edge-constraint nets. Our discrete surface representation via nets relates to [HSFW17], where however the normals were discretized differently. For a more systematic and detailed analysis of this discretization see [HY18]. Let $X = (V, F, E)$ be a discrete surface, where V, F and E denote the set of vertices, faces and edges. In the general case, the faces may be arbitrary oriented polygons; they need not be triangular or even planar. We denote the number of faces and vertices by $|F|$ and $\#V$ respectively.

Let $\mathcal{X} = (X, n)$ be a discrete surface as above, where additionally each face is assigned a unit vector $n : F \to S^2$. We will call the vector n_i at face i the *normal* at the face. $\mathcal{X}$ is called a *face edge-constrained net* if and only if, at every edge $e_{ij} \in E$, shared by its adjacent faces i and j, it holds that

$$n_i + n_j \perp e_{ij} \tag{8}$$

where n_i and n_j are the normals on the respective faces. We will refer to face edge-constrained nets as simply "nets" in the following.

In this setting, the bending angle θ_{ij} at each e_{ij} is defined by the angle between the planes P_i and P_j, where P_i is spanned by e_{ij} and n_i and P_j is spanned by e_{ij} and n_j. Note that Eq. (8) is always satisfied by any net whose faces are planar and where, for every face i, n_i is defined as the standard face normal perpendicular to the face plane. We call such nets *classical* nets. The bending angles for classical nets are just the angles between the face normals.

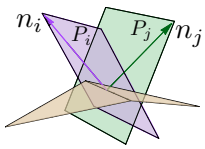

Curvature Definitions. The *integrated mean curvature* on a net edge is defined as $\mathbf{H}_{ij} := \frac{1}{2}|e_{ij}| \tan\frac{\theta_{ij}}{2}$ where θ_{ij} is the bending angle of the edge as above. The *integrated* mean curvature on a face i is defined as the sum of the mean curvature of the incident edges

$$\mathbf{H}_i = \sum_j \mathbf{H}_{ij} \tag{9}$$

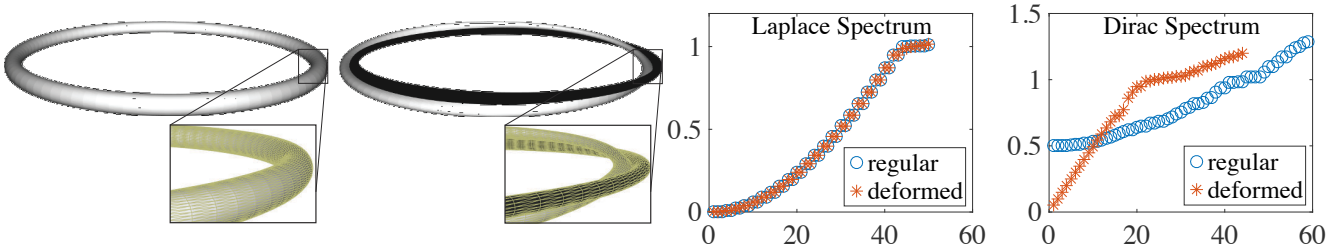

Figure 5: *Laplace-Beltrami and Dirac spectra of two tori, constructed to be approximately isometric but different in terms of their spin structure. The Laplace-Beltrami eigenvalues for the two tori are almost identical, given the approximate isometry. However, the Dirac eigenvalues help distinguish between the two.*

This choice of discretization of integrated curvature [KW14] is motivated by the Steiner formula for smooth immersed surfaces, which relates the infinitesimal area form dA of a surface X to the area form dA_t of an "offset" surface X_t. X_t is obtained by parallel offsetting every point of X along the normals by distance t. Then the Steiner formula states that $dA_t = (1+2Ht+Kt^2)dA$, where H and K stand for the mean curvature and Gauss curvature of X respectively (inset, top). For a triangulated surface, creating an offset face can be done by offsetting a face i along n_i, and all faces j adjacent to i along their respective normals n_j by the distance t (inset, bottom). It turns out that using the definition (9) one obtains a similar Steiner formula in the discrete case [KW14], where now dA is replaced by per-face areas. Even though, in general, such offsets do not exist for the whole surface, we formally define (9) as the integrated mean curvature for face edge-constraint nets. Note that, in order to be consistent with the terminology in [KPP98, CPS11], we choose the sign of H which is different from the one in [KW14].

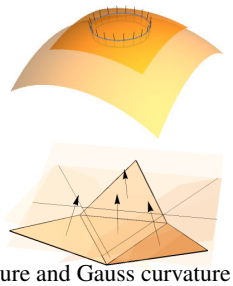

In the continuous case, the integrated mean curvature behaves like $\mathbf{H} = H|df|^2$, where $|df|^2$ the area form and H the mean curvature; the mean curvature half-density is, by definition (Section 3.2), $h := H|df|$. Accordingly, we define the discrete *mean curvature half-density* by

$$\mathbf{h}_i := \frac{\mathbf{H}_i}{\sqrt{\text{Area}_i}} \tag{10}$$

where Area_i corresponds to triangle area. Based on the mean curvature half-density, the *Willmore energy* W can be defined. In the continuous case, the energy is defined as $W = \int h^2$ [CPS11]. Based on this formula, we define the discrete Willmore energy using our discretized curvatures by

$$W := \sum_i \frac{\mathbf{H}_i^2}{\text{Area}_i} \tag{11}$$

In Fig. 2 we show Willmore energy calculations for discrete versions of surfaces for which the value of the energy is known in the continuous case, and find that the discrete energy values are close to the predicted ones. The figure also indicates that our discrete energy is numerically invariant to Möbius transformations, as expected.

4.2. Discrete Dirac Operators

Discrete extrinsic Dirac operator. Let $\mathcal{X} = (X, n)$ be a net. We associate every edge $e_{ij} \in E$ between triangles i and j with a quaternion $E_{ij} \in \mathbb{H}$, with real part equal to the integrated mean curvature $\mathbf{H}_{ij}$ at the edge, and imaginary part equal to the embedding e_{ij} of the edge in 3D space, viewed as an imaginary quaternion

$$E_{ij} = 2\mathbf{H}_{ij} + e_{ij} \tag{12}$$

We call this quaternion the *hyperedge* corresponding to $\mathbf{e}_{ij}$. It's easy to see that, for the inverse edge e_{ji}, $E_{ij} = \overline{E}_{ji}$. If the bending angle between faces i and j is zero, E_{ij} is pure imaginary and the hyperedge reduces to the edge.

Let $\Omega : F \to \mathbb{H}$ be the set of face-based quaternion-valued functions on our net. Since the extrinsic Dirac operator (2) can be reformulated as $D_f\phi = \langle df, *d\phi \rangle$, where $*$ is the Hodge star, we consider ϕ as a face-based function and define the *discrete extrinsic Dirac operator* as the $4|F| \times 4|F|$ sparse matrix such that

$$\begin{aligned} D_f &: \Omega \to \Omega \\ (D_f\phi)_i &= \frac{1}{2}\sum_j E_{ij}(\phi_j - \phi_i) = \frac{1}{2}\sum_j E_{ij}\cdot\phi_j - \mathbf{H}_i\phi_i \end{aligned} \tag{13}$$

The following theorem (proven in the appendix) shows that the discrete extrinsic Dirac operator relates to spin transformations (conformal integrable deformations) of discrete surfaces, with prescribed mean curvature half-density. This directly corresponds to the equivalent relation from the continuous case (Eq. (1)).

Theorem 4.1 Let $\phi \in \Omega$ be a per-face quaternion-valued function on a net satisfying the extrinsic Dirac equation

$$D_f\phi = \rho\phi \tag{14}$$

where $\rho : F \to \mathbb{R}$ is a face-based real valued function. When ϕ is applied as a transformation on the faces F of the net, it produces another immersed net, with hyperedges and normals as follows:

$$E_{ij} \mapsto \bar{\phi}_i \cdot E_{ij} \cdot \phi_j := \tilde{E}_{ij} \tag{15}$$

$$n_i \mapsto \phi_i^{-1} \cdot n_i \cdot \phi_i := \tilde{n}_i \tag{16}$$

Eq. (15) and (16) describe a *discrete spin transformation*. The integrated mean curvature of the new net is given by the discrete analogue of Eq. (3), namely

$$\tilde{\mathbf{H}}_i = (\rho_i + \mathbf{H}_i)|\phi_i|^2 \tag{17}$$

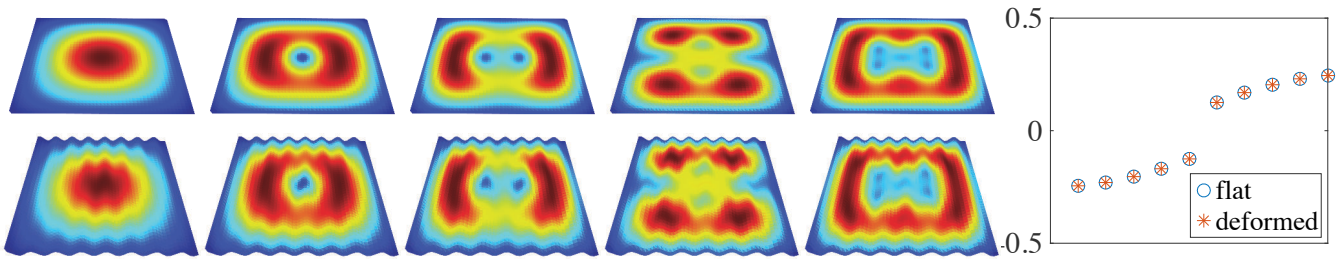

Figure 6: *Spectra of the discrete intrinsic Dirac operator for two isometric surfaces. The bottom mesh is the result of translating the vertices of the top planar mesh while keeping the edge lengths unchanged. The colors show the magnitude of the eigenfunctions corresponding to the first five eigenvalues for the two meshes. On the right, the plot shows the eigenvalues of the operator for the two meshes, which are identical.*

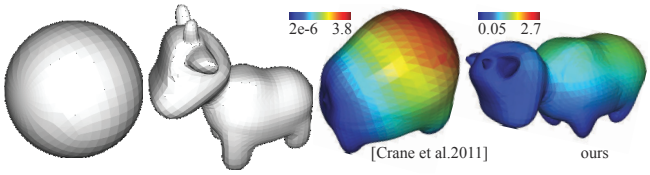

Figure 7: *Recovering a cow from a sphere using the mean curvature half-density to design a spin transformation.*

Minimal Surfaces. We call a net a *minimal surface*, if $\mathbf{H}_i = 0$ for all faces i. If ϕ is a solution of the Dirac equation

$$D_f\phi = -\mathbf{H}\phi \tag{18}$$

then from Eq. (17), the corresponding spin transformation gives a minimal surface. Analogously to the smooth case, a discrete minimal surface does not come alone but always in a family - if ϕ satisfies Eq. (18), a straightforward calculation (shown in the appendix) verifies that the quaternionic functions of the form $\phi(\lambda)|_i = (\cos\lambda + \sin\lambda n_i)\phi_i$ for some parameter λ all satisfy Eq. (18) as well. We showcase some discrete minimal surfaces in Fig. 3.

Discrete intrinsic Dirac operator. We define this operator by

$$(D\phi)_i = \frac{1}{2}\sum_j E_{ij}\cos\frac{\theta_{ij}}{2}\phi_j \tag{19}$$

Note the presence of an additional cosine factor. Without it, the operator would be *covariant* under transformations of the form

$$E_{ij} \mapsto \bar{g}_i \cdot E_{ij} \cdot g_j$$
$$n_i \mapsto g_i^{-1} \cdot n_i \cdot g_i$$

with $|g_i| = 1$. Such a transformation preserves the norm of the hyperedges $|E_{ij}|$; it does not, however, preserve edge lengths. Note also that the norm of the quaternion $E_{ij}\cos\frac{\phi_{ij}}{2}$ is the same as the edge length $|e_{ij}|$. Hence we introduce the cosine factor in this formula as a correction factor in the discrete case, to ensure the covariance under *edge-length preserving* deformations; we found that this produces much better results in practice. Similarly to the extrinsic case, we prove the equivalent of Eq.(6), regarding the relation between the intrinsic Dirac operator and conformal immersions, which now holds in the discrete case.

Theorem 4.2 Any $\phi \in \Omega$ satisfying the intrinsic Dirac equation

$$D\phi = \rho\phi \tag{20}$$

where $\rho : F \to \mathbb{R}$ is a face-based real valued function, gives another immersed edge-constraint net by the spin transformation:

$$E_{ij} \;\mapsto\; \cos\frac{\theta_{ij}}{2}\bar{\phi}_i \cdot E_{ij} \cdot \phi_j := \tilde{E}_{ij} \tag{21}$$
$$n_i \;\mapsto\; \phi_i^{-1} \cdot n_i \cdot \phi_i := \tilde{n}_i \tag{22}$$

The integrated mean curvature of the new surface is given by the discrete analogue of Eq. (7), namely

$$\tilde{\mathbf{H}}_i = \rho_i|\phi_i|^2 \tag{23}$$

The following theorem (proven in the appendix) shows that this discrete intrinsic Dirac operator is indeed intrinsic.

Theorem 4.3 The intrinsic Dirac operator in Eq. (19) is covariant under an isometric deformation and the extrinsic Dirac operator in Eq. (13) is covariant under a rigid transformation.

In fact it is possible to construct the intrinsic Dirac operator using only the metric (edge lengths) and some extra structure called the spinor connection, i.e. without knowing the vertex positions. Since all of the applications in this paper are based on immersed surfaces, we will not present the details on this process but refer the readers to [HY18]. Remarkably, in parallel to our work, a closely related spinor connection structure has been developed by Chern et al. [CKPS18] for the purposes of isometric shape embeddings.

4.3. Numerical methods

In this section we outline common numerical problems involving our Dirac operators that frequently appear in applications and experiments in the remainder of the paper. Note that both operators are symmetric matrices. This implies that the eigenvalues and eigenfunctions are always real-valued.

Spin transformations. Frequently, we need to prescribe a curvature potential $\rho : F \to \mathbb{R}$ on a given mesh and compute the spin transformation (per-face quaternion-valued function ϕ) that will deform the mesh so it obtains the prescribed mean curvature. For this we need to solve the Dirac equation of either Eq. (14) or Eq. (20) of the form $D\phi = \rho\phi$ with the prescribed ρ. Note, however, that the

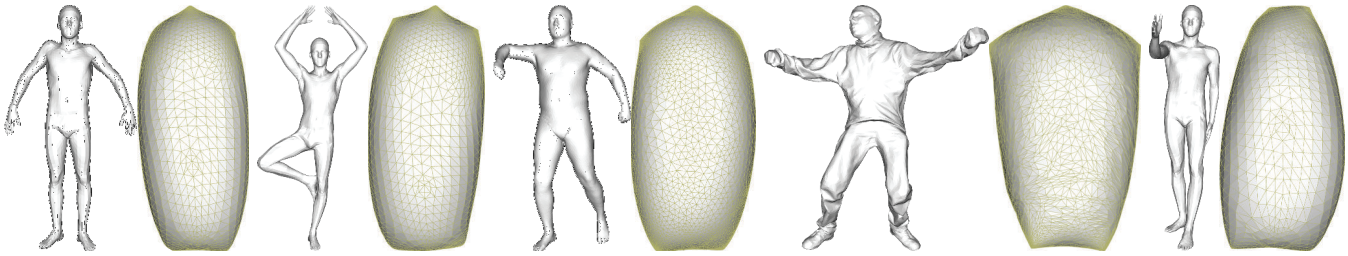

Figure 8: *The first Dirac humans. We compute the eigenfunction of our intrinsic Dirac operator corresponding to its smallest eigenvalue, and apply it as a spin transformation to deform the input human mesh. Note the similar appearance of the resulting surfaces.*

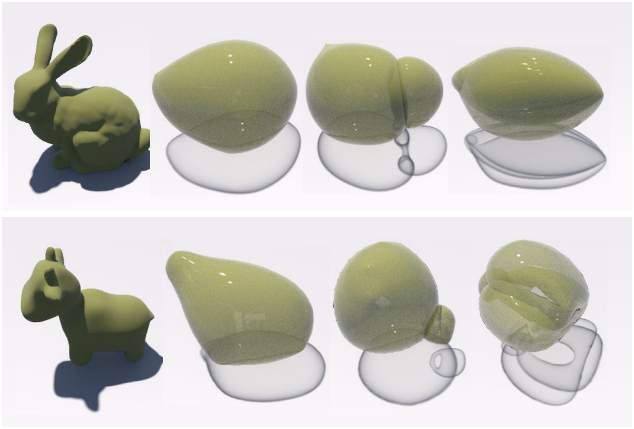

Figure 9: *Dirac animals. We compute the eigenfunctions of our intrinsic Dirac operator corresponding to its smallest eigenvalues, and apply them as a spin transformation to deform an input mesh.*

existence of the solution ϕ is not always guaranteed for all ρ. In order to solve for the transformation ϕ, we follow the same process as in [CPS11, Section 4] , namely we solve the following eigenvalue problem for an eigenvalue λ with small magnitude.

$$(D-\rho)\phi = \lambda\phi \tag{24}$$

Spectrum Calculations. In another common scenario, we wish to compute the eigenvalues and the eigenfunctions of the (intrinsic or extrinsic) Dirac operator

$$D\phi_i = \lambda_i\phi_i \tag{25}$$

where $\cdots \leq \lambda_{-1} \leq 0 \leq \lambda_1 \leq \cdots$. The recovered ϕ's may then be used for analysis, or as a spin transformation to deform a surface for the relevant application.

Numerical Considerations. Numerical experiments show that the computed ϕ_i's are smooth if the target ρ in Eq. (24) has a small magnitude or only few eigenfunctions are required in Eq. (25). As the magnitude of ρ increases or more eigenfunctions are needed, numerical instabilities with the face-based Dirac operator may create non-smooth solutions. In these cases, we use an additional face-to-vertex averaging matrix A (the $4|F| \times 4\#V$ incidence matrix) and solve the generalized eigenvalue problem

$$A^T \cdot \hat{D} \cdot M^{-1} \cdot \hat{D} \cdot A\phi = \lambda A^T \cdot \hat{D} \cdot A\phi \tag{26}$$

Here, M is the diagonal matrix with the face areas as entries, and $\hat{D} = D - P$, where P is a $4|F| \times 4|F|$ diagonal matrix containing the curvature information ρ as in (23) . If only eigenvalues of small magnitude are needed, we solve the simpler singular problem

$$A^T \cdot \hat{D} \cdot \hat{D} \cdot A\phi = \lambda A^T M \cdot A\phi. \tag{27}$$

Note that both these equations still only contain symmetric matrices on both sides, implying that the eigenvalues and eigenfunctions are always real-valued. After the ϕ's are computed, we use the transpose of the averaging matrix to compute a per-face quaternion function, which we can use for spin transformations if needed.

Deforming a surface with a spin transformation Given a spin transformation, we can compute the new surface by first applying the transformation to the hyperedges (Eq. (21)). We then recover the coordinates of the vertices by solving a linear system, similarly to [CPS11, Section 5.6]. Specifically, we collect the imaginary parts of the transformed hyperedges as the coordinates of the edge vectors (as per the definition Eq. (12)), and then solve the underdetermined sparse linear system

$$v_j - v_i = e_{ij}$$

for all the edges e_{ij}, where v_i, v_j are the vertices incident to e_{ij}. To solve this system we need to fix the coordinates of any one vertex. In practise, since numerical issues occurring during the Dirac eigenvalue problem might prevent this system from having an exact solution, we solve it in a least squares fashion, which we found yields satisfying results.

5. Evaluation and Analysis

In this section we validate our discrete operators against known properties of the continuous operators and evaluate their behaviour.

5.1. Spectrum verification

Eigenvalues on spheres. For the round unit sphere, the intrinsic Dirac operator eigenvalues are integers with multiplicity equal to their absolute value plus one, namely

$$\cdots, -3, -3, -3, -2, -2, -1, 1, 2, 2, 3, 3, 3, \cdots$$

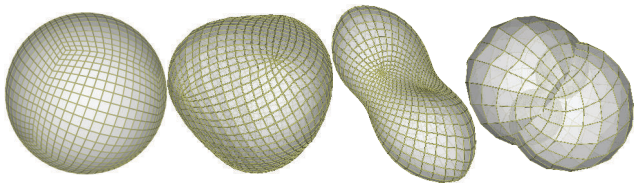

Figure 10: *Our intrinsic operator applied on a non-triangular mesh of a sphere (left). The middle two images show the spin transformations induces by setting ρ to equal the y euclidean coordinate at each point, and the product xyz respectively. The rightmost image shows the first Dirac immersion.*

Note that the intrinsic Dirac operator cannot have a zero eigenvalue on a sphere, since the corresponding spin transformation from Eq.(6) would result in a minimal sphere-topology surface with zero minimal curvature, which is impossible. In contrast, the extrinsic Dirac does have a zero eigenvalue, corresponding to eigenfunctions that are rigid transformations. We verify our discretization by performing eigenanalysis, using Eq. (26), on our intrinsic Dirac operator on various meshes of the unit sphere. We use various triangulations of different resolution, element quality, regularity and meshing types. Fig. 4 shows that our discrete operator gives exactly the same spectra regardless of meshing.

Eigenvalues on tori. The Dirac operator can be used to distinguish between surfaces that are isometric but have different *spin structure*. The spin structure of Riemannian manifolds is an abstract notion. However, in the case where an immersion $\mathbb{R}^3$ is available, it is more intuitive to understand: two surfaces have the same spin structure iff they are related by a regular homotopy [Pin85]. All simply-connected surfaces have a single spin structure; in the case of tori, 4 different spin structures exist. In Fig. 5 we construct two tori that are approximately isometric but differ in spin structure. To this end, we create the tori with the same radii in such a way that the big radius is much larger than the small one. In this way, both tori look locally like a flat cylinder, and are therefore approximately isometric. As shown in the figure, the two tori are indistinguishable in terms of the eigenvalues of their Laplace-Beltrami operators, due to the approximate isometry. On the other hand, they can be clearly distinguished based on the Dirac operator eigenvalues.

Invariance to isometries. In order to verify that our discrete intrinsic Dirac operator is indeed invariant under isometric deformations, we construct a simple experiment based on a planar mesh (Fig. 6). By displacing the vertices of the mesh while keeping the edge length unchanged, we obtain a non-planar mesh that is an isometric deformation of the original plane. As can be seen from the figure, both the eigenvalues and the patterns of the norm of eigenfunctions are unaffected by the deformation.

5.2. Recovering a conformal immersion

As noted in [KPP98] and [Cra13], apart from some extreme cases, the mean curvature half-density actually determines the conformal immersion that describes the embedding of a surface in $\mathbb{R}^3$. We validate this statement for the case of our discrete operators in Fig. 7,

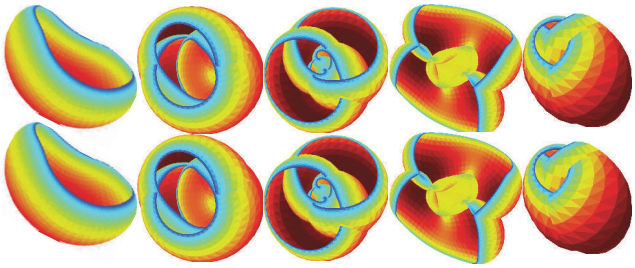

Figure 11: *The Dirac eigenfunctions of the two isometric surfaces of Fig. 6 applied as spin transformations onto their corresponding surfaces. Note that they are identical up to a rigid transformation. In pseudocolor, the magnitude of the corresponding eigenfunctions.*

by "extruding" a target mesh from a mesh of a unit sphere. In order to achieve this, we first compute the mean curvature half-density of the target mesh using Eq. (10), namely $\rho_i^{\text{target}} = \mathbf{H}_i^{\text{target}} / \sqrt{A_i^{\text{target}}}$, where A_i^{target} is the face area on the target mesh. Since this is an integrated quantity, we adapt it for the sphere mesh by $\rho_i = \rho_i^{\text{target}} \sqrt{A_i^{\text{sphere}}}$, and prescribe it as ρ in Eq. (20). We then compute the resulting spin transformation using equation Eq. (27) and apply it onto the spherical mesh. For comparison, in Fig. 7 we also show the result using the discrete extrinsic Dirac operator of Crane et al. [CPS11]. Note that since the operator in [CPS11] is extrinsic, we need to use the *difference* between the target mean curvature half-density and the mean curvature half-density of the sphere as the ρ in Eq. (1). Our discretization seems to be recovering the target surface more faithfully.

5.3. Dirac immersions

By *Dirac immersions* we refer to the conformal immersions that correspond to the intrinsic Dirac eigenfunctions. In [CPS11] such immersions (the *Dirac spheres*) were computed and visualized for the unit round sphere, for which closed-form expressions are known [Ric97] and find applications in physics. Note that the operator in [CPS11] is extrinsic and cannot be used to compute Dirac immersion for general surfaces – however, since the round sphere is of constant mean curvature $H = 1$, and using Eq. (5), it can be seen that the extrinsic and intrinsic Dirac operator only differ by a constant 1 in this case. Therefore, for the special case of a unit round sphere, one can extract the intrinsic Dirac eigenfunctions from the extrinsic Dirac eigenfunctions. Our purely intrinsic Dirac operator can be computed for any mesh – solving the eigenvalue problem (26) then allows us to directly visualize Dirac immersions of various degrees for arbitrary simply-connected surfaces (Fig. 9 and 8). Notably, the first Dirac immersions of the various human meshes are of similar shape, which might be of interest in applications.

Fast surface fairing. In the continuous case, the following theorem can be proven (see appendix):

Theorem 5.1 Let $f : M \to \mathbb{R}^3$ be the simply-connected immersed surface with Willmore energy W, and f_1 the immersion corresponding the Dirac eigenfunction with smallest eigenvalue. Then we have $W_1 \leq W$, where W_1 is the Willmore energy of f_1.

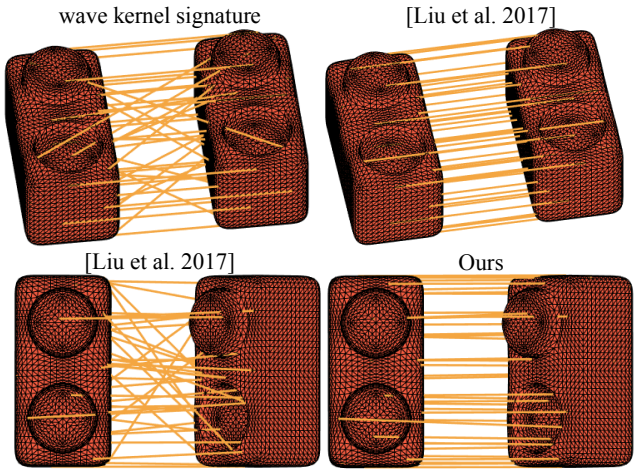

Figure 12: *Point-to-point correspondence between isometrically identical surfaces with different meshes. The Laplace-Beltrami-based wave kernel signature fails to differentiate between the inward and outward bumps. The Dirac kernel signature based on [LJC17] captures these extrinsically different features, but yields poor matches when one of the objects is slightly rotated. The same descriptor based on our operator overcomes both problems.*

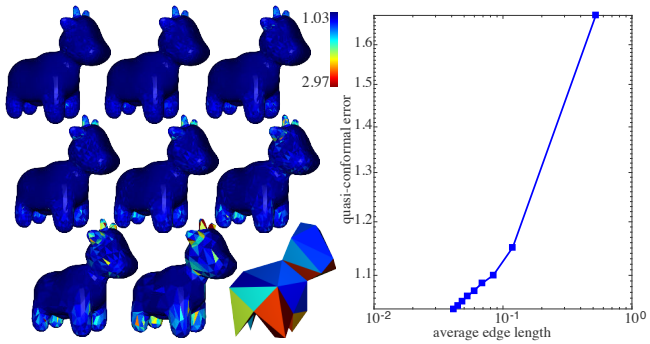

Figure 13: *On the left, the spatial distribution of the quasi-conformal errors between the original shape and its first Dirac immersion for different mesh resolutions. On the right, the average quasi-conformal error for different mesh resolutions, plotted against the average edge length.*

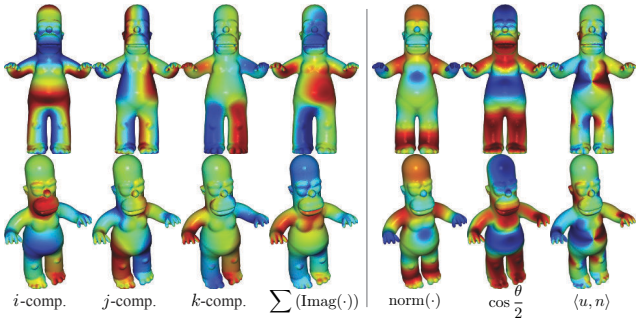

Figure 14: *Various quantities derived from the intrinsic Dirac eigenfunctions that vary (left) or remain invariant (right) under rigid transformations of an input mesh.*

Namely, the first Dirac immersion is always of lower Willmore energy than the initial surface, and thus smoother. This is also reflected in our discrete results. We can use this fact to rapidly transition from the surface to the round sphere in only a few steps, as shown in Fig. 15. We do this by repeatedly applying the spin transformation (Eq. (26)) corresponding to the first eigenfunction and recomputing the operator at each iteration.

Polygonal meshes. While our work mainly targets triangular meshes, we show some preliminary support for polygonal meshes – Fig. 10 shows simple curvature painting and a Dirac immersion for discrete spheres discretized as quadrilateral meshes.

Dirac immersions and isometries. The Dirac immersions of two isometric surfaces only differ by an Euclidean motion, as expected by the invariance of the eigenfunctions, shown in the proof of Theorem 4.3. We verify this statement for the two isometric surfaces of Fig. 6 : Fig. 11 shows the first few immersions for the plane (top) and its isometric deformation (bottom). The colors show the magnitude of the first five eigenfunctions for the two meshes, indicating the invariance of the immersions to isometries.

Comparison to Crane et al. [CPS13], [CPS11]. One can apply the formula $D = D_f + H$ on the discretization in [CPS11] and obtain another discrete intrinsic Dirac operator. Indeed, in some circumstances this operator gives similar results for regular meshes. However, due to the lack of invariant properties (see Theorem 4.3), it is more sensitive to the meshing than ours, see Fig. 17.

Our fast surface fairing looks very similar to Crane et al.'s conformal Willmore flow [CPS13] with time step $\frac{1}{2}$. However, for Willmore flow the potential needs to be projected onto the feasible space in order to ensure the existence of a solution [CPS13, Section 6.2]. With a relatively big time step this projection might not be effective and produce unexpected shapes, especially for complicated meshes. In contrast, it is guaranteed by our Theorem 5.1 that the first Dirac immersion will always reduce the Willmore energy. A drawback of our fast fairing approach is that it only works for simply-connected surfaces. The fine-grained, per-iteration control of the conformal Willmore flow in [CPS13], necessary to ensure global integrability, allows instead for practical applicability of this flow also to surfaces of higher genus.

5.4. Invariant properties.

Inspired by the widespread usage of the eigenfunctions of the Laplacian operator in shape analysis, a natural question might be whether it is possible to similarly extract geometric information from the Dirac eigenfunctions as well. For example, one might consider using the intrinsic Dirac operator for spectral feature extraction, similarly to HKS/WKS [SOG09, ASC11]. Additionally, as argued in [LJC17], some applications might benefit from intrinsicness of the respective operator, while others might require extrinsicness, e.g. when different kinds of symmetries need to be extracted. So a natural question that arises is, which geometric quan-

tities extracted from the intrinsic Dirac eigenfunctions are *intrinsic*, namely invariant under general isometric deformations, and which are *extrinsic* – which in this context means invariant under only rigid transformations. Such considerations affect the quality of the extracted descriptors and determine their potential for applications.

For example, the individual components of the quaternions corresponding to the intrinsic Dirac eigenfunctions (when viewed as $\mathbb{R}^4$) do not produce intrinsic quantities. Fig. 14 shows that, even under the canonicalization process of [LJC17], the individual quaternion components are still not invariant even under rigid transformation. In the appendix, we show that the per-face norm $|\phi_i|$ of the intrinsic Dirac eigenfunctions is an intrinsic quantity. Furthermore, the Dirac eigenfunctions contain two more extrinsic quantities, which are not available from the Laplacian eigenfunctions, as per the following theorem (proven in the appendix). That shows that the Dirac eigenfunctions reflect the extrinsic information, even though one uses the intrinsic Dirac operator.

Theorem 5.2 Let ϕ be the the eigenfunctions of extrinsic or intrinsic Dirac operator. At each face, we write $\phi_i = |\phi_i|\left(\cos\frac{\theta_i}{2} + \frac{\sin\theta_i}{2}u_i\right)$. The following two quantities are invariant under the rigid transformation:

- The rotation angle, or the normalized real part, $\cos\frac{\theta_i}{2}$.
- The angle between the rotation axis and the face normal $\langle u_i, n_i\rangle$.

Following the idea in [LJC17], we construct the shape descriptors, in the framework as the wave kernel signature [ASC11], based on the norm of Dirac eigenfunctions and two quantities above. The norm contributes to detecting the intrinsic geometric features, while the other two quantities are responsible for disambiguating the features, which are intrinsically similar but extrinsically different. The Dirac kernel signature in [LJC17] succeeds in detecting the extrinsically different features, however, it suffers from not being invariant under rigid transformations, because it contains the quantity, the sum over four quaternion components of the eigenfunctions, which varies under Euclidean motions. Since all of the quantities we used are invariant under rigid transformations, Fig. 12 shows that our shape descriptor fixes this problem.

Although our intrinsic Dirac operator is invariant under edge-length-preserving deformations, it is, in general, not invariant to different tessellations of the same surface. In the top inset figure, we consider two meshes inscribed in the unit sphere: one is a subdivided icosahedron (first from left), and the other is obtained by flipping the edges of the first (second from right). Note that the Dirac eigenvalues and Willmore energy of the first mesh are close to their predicted values; this is less so for the second mesh. Additionally, performing Willmore flow / fast fairing does not affect the first mesh (second from left); but doing the same on the second mesh decreases its Willmore energy (first from right). The change on the mesh is hardly noticeable though, implying that our operator remains stable for this second mesh. However, if the input is a mesh, still inscribed in the unit sphere but with a significantly worse normal approximation (bottom inset), fast fairing can become unstable. In this case, it first reduces the Willmore energy (bottom-middle); later the result becomes unstable and its Willmore energy grows uncontrollably. Improving our intrinsic operator to deal with such meshes with extremely bad normal approximation remains an avenue for future work.

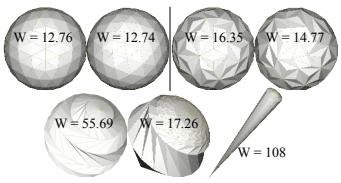

Comparison to Liu et al. In [LJC17], the relative Dirac operator is constructed by extracting the extrinsic part of the square of the extrinsic Dirac operator of [CPS11]. This modified operator, while being purely extrinsic, does not relate to spin transformations via Eq. (6) – neither does the intrinsic operator of [LJC17], which is essentially a quaternionic Laplacian. In that sense, our operators are more faithful to the continuous Dirac operator; Liu et al.'s operator cannot be used to compute spin transformations or immersions, for example. On the other hand, since the square of the [CPS11] operator also involves the Laplacian component, the relative Dirac operator can be thought of as the extrinsic Dirac operator without the impact of the Laplacian. Hence it is possibly "more extrinsic" than the operator of [CPS11] or ours, which might be interesting to consider in applications.

Our operators could possibly be applied to feature extraction using heat/wave kernel signatures (HKS/WKS), by using the norm of the Dirac eigenfunctions as opposed to Laplace-Beltrami. Our preliminary experiments in shape matching on state-of-the-art databases, however, do not show an obvious advantage in using our operator. We conjecture that the information contained in the *norm* of the Dirac eigenfunctions is equivalent to that of Laplace-Beltrami, and it is sufficient for these purely intrinsic shape matching experiments. Extract additional intrinsic scalar-valued information from the Dirac operator remains an interesting research topic.

5.5. Close-to-conformal spectral shape decomposition

In [VL08], the eigenfunctions of the Laplace-Beltrami operator were used to decompose a shape. This was done by projecting the vertex coordinate functions onto a truncated set of Dirac eigenfunctions of increasing eigenvalue magnitude; owing to the relation between the Laplacian and Fourier frequency analysis, using less eigenfunctions generally produces smoother versions of the input surface. In a similar fashion, we can now use the eigenfunctions of the Dirac operator, which will produce a close-to-conformal decomposition. To this end, we can represent the input shape as the identity quaternionic transformation with the constant value $\phi = (1,1,\ldots,1)$ on all faces and project this function onto a subset of the Dirac eigenfunctions (Eq. (26)). We then apply the reconstructed sum as a spin transformation on the original surface. The results are shown in Fig. 16. Note that the weighted sum of a truncated Dirac eigenfunction basis does not produce an integrable spin transformation in general – while we did not find this to be a problem in practise, an additional projection step could be applied to ensure integrability if necessary.

5.6. Convergence under different meshings.

Following [CPS11], we use the quasi-conformal error [SSGH01] to measure the quality of our conformal mappings. At each face,

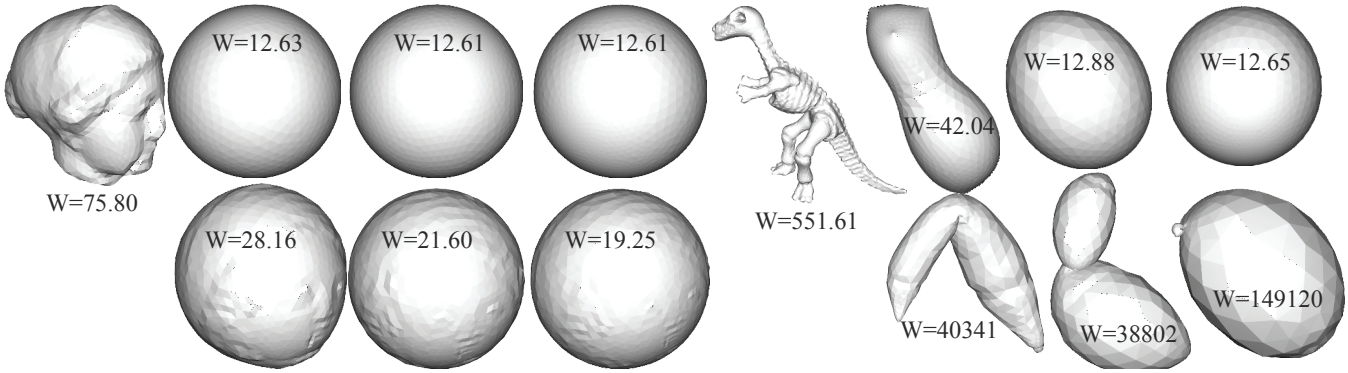

Figure 15: *For each mesh, the top row shows the results of iteratively applying the first Dirac eigenfunction as a spin transformation. This produces a progressively smoother shape, as reflected by the reduced Willmore energy values. The bottom row shows, for the same meshes, the application of conformal Willmore flow with a big time step $\frac{1}{2}$. Note that while both techniques work for the first shape, which deforms fast towards the round sphere, the conformal Willmore flow with big time step is quite unstable for the second shape.*

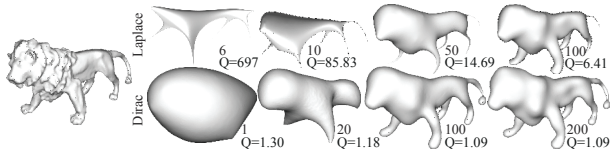

Figure 16: *Top: the classical spectral decomposition of a mesh, using Laplace-Beltrami eigenfunctions. Bottom: close to conformal decomposition using intrinsic Dirac eigenfunctions; the first shape here is the first Dirac immersion. We plot the quasi-conformal distortion [SSGH01] induced by the low-pass filtering, which is much smaller using our method. Note that we generally use twice as many Dirac eigenfunctions (counted by quaternionic multiplicity) as Laplace eigenfunctions, since the intrinsic Dirac operator always has symmetric eigenvalues* $\{\lambda_1, -\lambda_1, \lambda_2, -\lambda_2, \ldots\}$.

we compute the ratio Q_i between the largest and smallest singular value of the differential df. The ideal value is $Q_i = 1$, implying that the map is uniform scaling and rotation. We compute the total error Q for a surface by averaging the quasi-conformal errors per face using area weighting. Fig. 13 shows that the quasi-conformal error between a shape and its first Dirac immersion goes to 1 as the average edge-length goes to zero. Additionally, Fig. 16 and Fig. 17 show that our method generally induces low quasi-conformal error.

6. Conclusion

We presented a new discretization framework for the Dirac operator on discrete surface meshes. Our framework allows for the discretization of both an extrinsic and an intrinsic Dirac operator, both of which are in alignment with their continuous counterparts in their basic properties. Most importantly, they both relate to integrable conformal deformations, which is a fundamental property of the continuous operator.

Exploring more applications of these discrete operators is a natural avenue for future work. In particular, it might be interesting to investigate whether a spectrum of operators, with various degrees of "intrinsicness" can be constructed, similarly to [LJC17]. Additionally, the space of quaternionic-valued functions might provide an interesting domain for constructing mappings between shapes, transferring shape deformations, or defining shape features. Understanding the role of intrinsicness vs. extrinsicness in applications, and knowing what kind of geometric properties can be captured by these operators is an interesting topic to study, which hopefully will be aided by our unified discretization framework. Besides, even though Fig. 17 and Fig. 4 show that our Dirac operator is practically stable, a systematic stability analysis, for instance within the finite element scheme, is one of our goals for future research.

Acknowledgements: This work was supported by the Swiss National Foundation Early PostDoc. Mobility Grant P2EZP2-165215, the DFG-Collaborative Research Center, TRR 109, "Discretization in Geometry and Dynamics", NSF grants IIS-1528025 and DMS-1546206, a Google Focused Research award, and gifts from Adobe, Amazon and NVIDIA.

References

[ABCCO13] AZENCOT O., BEN-CHEN M., CHAZAL F., OVSJANIKOV M.: An operator approach to tangent vector field processing. In *Proceedings of the Eleventh Eurographics/ACMSIGGRAPH Symposium on Geometry Processing* (Aire-la-Ville, Switzerland, Switzerland, 2013), SGP '13, Eurographics Association, pp. 73–82. 2

[ACBCO17] AZENCOT O., CORMAN E., BEN-CHEN M., OVSJANIKOV M.: Consistent functional cross field design for mesh quadrangulation. *ACM Trans. Graph. 36*, 4 (July 2017), 92:1–92:13. 2

[AOCBC15] AZENCOT O., OVSJANIKOV M., CHAZAL F., BEN-CHEN M.: Discrete derivatives of vector fields on surfaces – an operator approach. *ACM Trans. Graph. 34*, 3 (May 2015), 29:1–29:13. 2

[AS63] ATIYAH M. F., SINGER I. M.: The index of elliptic operators on compact manifolds. *Bulletin of the American Mathematical Society 69* (1963), 422–433. 2

[ASC11] AUBRY M., SCHLICKEWEI U., CREMERS D.: The wave kernel signature: A quantum mechanical approach to shape analysis. In *2011 IEEE International Conference on Computer Vision Workshops (ICCV Workshops)* (Nov 2011), pp. 1626–1633. 2, 9, 10

[Bär96] BÄR C.: The dirac operator on space forms of positive curvature. *Journal of the Mathematical Society of Japan 48*, 1 (jan 1996), 69–83.

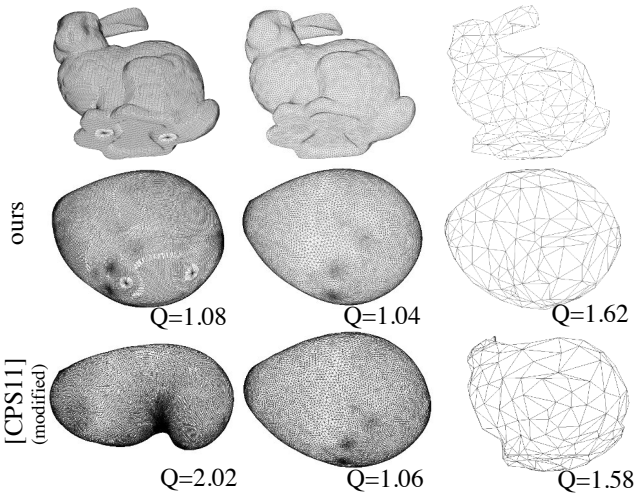

Figure 17: *The Dirac bunnies with different meshings. Top row, left to right: the original bunny mesh, an isotropic remeshing and a highly simplified mesh. Middle row: the Dirac immersions for these meshes using our operator. The output shapes are of very similar appearance despite the very different input tesselations. Bottom row: the immersions produced via the modified version of the operator in [CPS11], i.e., $D = D_f + H$. In contrast to our result, these differ significantly in appearance for the different inputs.*

[Bär98] BÄR C.: Extrinsic bounds for eigenvalues of the dirac operator. *Annals of Global Analysis and Geometry 16*, 6 (Dec 1998), 573–596. 14

[BS05] BOBENKO A. I., SCHRÖDER P.: Discrete willmore flow. In *Proceedings of the Third Eurographics Symposium on Geometry Processing* (Aire-la-Ville, Switzerland, Switzerland, 2005), SGP '05, Eurographics Association.

[Chu16] CHUBELASCHWILI D.: *Variational Formulas for Immersions Into 3-manifolds*. Master's thesis, Technische Universitaet Berlin, 2016. 4

[CKPS18] CHERN A., KNÖPPEL F., PINKALL U., SCHRÖDER P.: Shape from metric. *ACM Trans. Graph. 37*, 4 (August 2018), 63:1–63:17. 6

[Cno02] CNOPS J.: *An Introduction to Dirac Operators on Manifolds*. An Introduction to Dirac Operators on Manifolds. SPRINGER VERLAG NY, 2002. 4

[CPS11] CRANE K., PINKALL U., SCHRÖDER P.: Spin transformations of discrete surfaces. *ACM Trans. Graph. 30*, 4 (2011), 104. 1, 2, 3, 5, 7, 8, 9, 10, 12

[CPS13] CRANE K., PINKALL U., SCHRÖDER P.: Robust fairing via conformal curvature flow. *ACM Trans. Graph. 32* (2013). 3, 9

[CPS15] CHERN A., PINKALL U., SCHRÖDER P.: Close-to-conformal deformations of volumes. *ACM Trans. Graph. 34*, 4 (July 2015), 56:1–56:13.

[Cra13] CRANE K.: *Conformal Geometry Processing*. PhD thesis, Caltech, June 2013. 1, 8

[CSBC*17] CORMAN E., SOLOMON J., BEN-CHEN M., GUIBAS L., OVSJANIKOV M.: Functional characterization of intrinsic and extrinsic geometry. *ACM Trans. Graph. 36*, 2 (Mar. 2017), 14:1–14:17. 1

[DRW10] DEY T. K., RANJAN P., WANG Y.: Convergence, stability, and discrete approximation of laplace spectra. In *Proceedings of the Twenty-first Annual ACM-SIAM Symposium on Discrete Algorithms* (Philadelphia, PA, USA, 2010), SODA '10, Society for Industrial and Applied Mathematics, pp. 650–663. 2

[Esp98] ESPOSITO G.: *Dirac Operators and Spectral Geometry*. Cambridge Lecture Notes in Physics. Cambridge University Press, 1998. 2

[Fri98] FRIEDRICH T.: On the spinor representation of surfaces in euclidean 3-space. *Journal of Geometry and Physics 28*, 1 (1998), 143 – 157. 4

[Gin09] GINOUX N.: *The Dirac Spectrum*. Springer Berlin Heidelberg, 2009. 2

[HKA15] HERHOLZ P., KYPRIANIDIS J. E., ALEXA M.: Perfect laplacians for polygon meshes. In *Proceedings of the Eurographics Symposium on Geometry Processing* (Aire-la-Ville, Switzerland, Switzerland, 2015), SGP '15, Eurographics Association, pp. 211–218. 2

[HSFW17] HOFFMANN T., SAGEMAN-FURNAS A. O., WARDETZKY M.: A discrete parametrized surface theory in $\mathbb{R}^3$. *International Mathematics Research Notices 2017*, 14 (2017), 4217–4258. 4

[HSTP11] HILDEBRANDT K., SCHULZ C., TYCOWICZ C. V., POLTHIER K.: Interactive surface modeling using modal analysis. *ACM Trans. Graph. 30*, 5 (Oct. 2011), 119:1–119:11. 2

[HY18] HOFFMANN T., YE Z.: A discrete extrinsic and intrinsic Dirac operator. *ArXiv e-prints* (Feb. 2018). 4, 6

[Kam02] KAMBEROV G.: *Quaternions, Spinors, and Surfaces*. Contemporary mathematics - American Mathematical Society. American Mathematical Society, 2002. 2

[KCPS15] KNÖPPEL F., CRANE K., PINKALL U., SCHRÖDER P.: Stripe patterns on surfaces. *ACM Trans. Graph. 34*, 4 (July 2015), 39:1–39:11.

[KJP*18] KOSTRIKOV I., JIANG Z., PANOZZO D., ZORIN D., BRUNA J.: Surface networks. In *The IEEE Conference on Computer Vision and Pattern Recognition (CVPR)* (June 2018). 3

[KPP98] KAMBEROV G., PEDIT F., PINKALL U.: Bonnet pairs and isothermic surfaces. *Duke Math. J. 92*, 3 (04 1998), 637–644. 2, 3, 5, 8

[KW14] KARPENKOV O., WALLNER J.: On offsets and curvatures for discrete and semidiscrete surfaces. *Beiträge zur Algebra und Geometrie / Contributions to Algebra and Geometry 55*, 1 (Mar 2014), 207–228. 5

[LHJ*14] LING R., HUANG J., JÜTTLER B., SUN F., BAO H., WANG W.: Spectral quadrangulation with feature curve alignment and element size control. *ACM Trans. Graph. 34*, 1 (Dec. 2014), 11:1–11:11. 2

[LJC17] LIU D., JACOBSON A., CRANE K.: A dirac operator for extrinsic shape analysis. *Computer Graphics Forum (SGP) 36*, 5 (2017). 1, 3, 9, 10, 11, 14

[LM16] LAWSON H., MICHELSOHN M.: *Spin Geometry (PMS-38)*. Princeton Mathematical Series. Princeton University Press, 2016. 4

[LP18] LAM W. Y., PINKALL U.: Infinitesimal conformal deformations of triangulated surfaces in space. *Discrete & Computational Geometry* (may 2018). 3

[LRF10] LIPMAN Y., RUSTAMOV R. M., FUNKHOUSER T. A.: Biharmonic distance. *ACM Trans. Graph. 29*, 3 (July 2010), 27:1–27:11. 2

[LS16] LEOPARDI P., STERN A.: The abstract hodge–dirac operator and its stable discretization. *SIAM Journal on Numerical Analysis 54*, 6 (jan 2016), 3258–3279. 3

[LZ10] LÉVY B., ZHANG H. R.: Spectral mesh processing. In *ACM SIGGRAPH 2010 Courses* (New York, NY, USA, 2010), SIGGRAPH '10, ACM, pp. 8:1–8:312. 1, 2

[OBCS*12] OVSJANIKOV M., BEN-CHEN M., SOLOMON J., BUTSCHER A., GUIBAS L.: Functional maps: A flexible representation of maps between shapes. *ACM Trans. Graph. 31*, 4 (July 2012), 30:1–30:11. 2

[Pin85] PINKALL U.: Regular homotopy classes of immersed surfaces. *Topology 24*, 4 (1985), 421–434. 8

[Ric97] RICHTER J.: *Conformal maps of a Riemannian surface into the space of quaternions.* Berlin: TU Berlin, FB Mathematik, 1997. 8

[Rus10] RUSTAMOV R. M.: Robust volumetric shape descriptor. In *Proceedings of the 3rd Eurographics Conference on 3D Object Retrieval* (Aire-la-Ville, Switzerland, Switzerland, 2010), 3DOR '10, Eurographics Association, pp. 1–5. 2

[SOG09] SUN J., OVSJANIKOV M., GUIBAS L.: A concise and provably informative multi-scale signature based on heat diffusion. In *Proceedings of the Symposium on Geometry Processing* (Aire-la-Ville, Switzerland, Switzerland, 2009), SGP '09, Eurographics Association, pp. 1383–1392. 2, 9

[SSGH01] SANDER P. V., SNYDER J., GORTLER S. J., HOPPE H.: Texture mapping progressive meshes. In *Proceedings of the 28th Annual Conference on Computer Graphics and Interactive Techniques* (New York, NY, USA, 2001), SIGGRAPH '01, ACM, pp. 409–416. 10, 11

[VL08] VALLET B., LÉVY B.: Spectral geometry processing with manifold harmonics. *Computer Graphics Forum 27*, 2 (apr 2008), 251–260. 10

Appendix A: Proofs

In this section we outline proofs to the theorems presented in the main portion of the paper.

Proof of Theorem 4.1. To prove integrability of the transformation, we need to show that the transformed edges (Eq. (15)) close up around each face. Indeed, summing up the transformed hyperedges around each face we obtain

$$\begin{aligned}\sum_j \bar{\phi}_i \cdot E_{ij} \cdot \phi_j &= \bar{\phi}_i \cdot (\sum_j E_{ij} \cdot \phi_j) \\ &= \bar{\phi}_i \cdot 2(\mathbf{H}_i + \rho_i) \cdot \phi_i \\ &= 2(\mathbf{H}_i + \rho_i)|\phi_i|^2 \end{aligned} \tag{28}$$

We used the Dirac operator definition (13) for the second equality and and the spin transformation condition (14) for the third. The result above is a real number - recall that the imaginary part of the hyperedges corresponds to the edge vector. Since the imaginary part vanishes, the transformed edges indeed close around each face. Thus the transformed surface closes up.

We now still need to prove that the resulting surface is a face edge-constrained net. We first prove the intermediate result that a discrete net with prescribed normals (X, n) satisfies the edge-constraint (8) if and only if we can associate each edge with a hyperedge E_{ij} such that

$$E_{ij}^{-1} \cdot n_i \cdot E_{ij} = -n_j. \tag{29}$$

- Assume Eq. (8) holds, and we have defined the hyperedges on the net as in the main text (Eq.(12)). Then

$$\begin{aligned} E_{ij} &= \tan\frac{\theta_{ij}}{2}|e_{ij}| + e_{ij} \\ &= \frac{|e_{ij}|}{\cos\frac{\theta_{ij}}{2}}\left(\sin\frac{\theta_{ij}}{2} + \cos\frac{\theta_{ij}}{2}\frac{e_{ij}}{|e_{ij}|}\right) \\ &= -\frac{|e_{ij}|}{\cos\frac{\theta_{ij}}{2}}\left(\cos\frac{\theta_{ij}+\pi}{2} - \sin\frac{\theta_{ij}+\pi}{2}\frac{e_{ij}}{|e_{ij}|}\right) \end{aligned} \tag{30}$$

  and hence n_i will be transformed to $-n_j$ with the rotation E_{ij}, and thus Eq. (29) holds.

- Assume there exists a hyperedge E_{ij} such that Eq. (29) holds for two normals n_i and n_j. Then, E_{ij} rotates n_i to $-n_j$, and the rotation axis is $e_{ij} := \mathrm{Im}(E_{ij})$. This means that the projections of n_i and $-n_j$ onto e_{ij} are equal, and thus $(n_i + n_j) \cdot e_{ij} = 0$, or $(n_i + n_j) \perp e_{ij}$. This proves the intermediate result.

Now, assume the spin transformation maps E_{ij} to $\tilde{E}_{ij}$ and n_i to $\tilde{n}_i$. Then we obtain

$$\tilde{E}_{ij}^{-1} \cdot \tilde{n}_i \cdot \tilde{E}_{ij} = \phi_j^{-1} E_{ij}^{-1} \bar{\phi}_i^{-1} \cdot \phi_i^{-1} n_i \phi_i \cdot \bar{\phi}_i E_{ij} \phi_j = -\bar{\phi}_j^{-1} n_j \phi_j = -\tilde{n}_j$$

and thus Eq. (29) holds. Therefore the spin transformation maps an edge-constraint net to an edge-constraint net.

By definition, the real parts of a hyperedge is the edge-integrated mean curvature. Then, the sum of the real parts of the transformed hyperedges is actually (Eq. (9)) the per-face integrated curvature of the new net. This sum is exactly the result of the summation above, since the imaginary part vanishes. This proves (17) and concludes the theorem.

The associated family of minimal surfaces. Given any immersed net f, a minimal surface is obtained by solving the equation

$$(D_f \phi)_i = -\mathbf{H}_i \phi_i$$

which in our discretization translates to

$$\sum_j E_{ij} \cdot \phi_j = 0 \tag{31}$$

Assuming that a solution ϕ exists, we insert the quaternion-valued function $\phi(\lambda)|_i = (\cos\lambda + \sin\lambda n_i)\phi_i$ into Eq. (31):

$$\sum_j E_{ij} \cdot \phi(\lambda)|_j = \sum_j \left(\cos\lambda E_{ij}\phi_j + \sin\lambda E_{ij} n_j \phi_j\right) = \sum_j \sin\lambda E_{ij} n_j \phi_j$$

since ϕ is minimal. From Eq. (29), we have $E_{ij} n_j = -n_i E_{ij}$. Thus

$$\sum_j E_{ij} \cdot \phi(\lambda)_j = -\sum_j \sin\lambda n_i E_{ij} \phi_j = -\sin\lambda n_i \sum_j E_{ij}\phi_j = 0$$

and all $\phi(\lambda)$ induce minimal surfaces.

Proof of Theorem 4.2 Again, we sum up the transformed hyperedges around each face:

$$\bar{\phi}_i \cdot (\sum_j \cos\frac{\theta_{ij}}{2} E_{ij} \cdot \phi_i) = 2\bar{\phi}_i \cdot (\rho_i) \cdot \phi_i = 2\rho_i |\phi_i|^2$$

and notice that the imaginary part vanishes. The remainder of the proof is identical to the proof of Theorem 4.1.

Proof of Theorem 4.3. Let $h_{ij} \in \mathbb{H}$ be the unit quaternion which rotates n_i to n_j. Then we can define the modified hyperedges $\mathcal{E}_{ij} := \cos\frac{\theta}{2} E_{ij} = e_{ij} \cdot h_{ij}$, which are used in the intrinsic Dirac operator. Now, assume that two classical nets $\mathcal{X}$ and $\tilde{\mathcal{X}}$ are related by an isometric deformation. This means that we will have $e_{ij} = g_i^{-1} \tilde{e}_{ij} g_i$ and $h_{ij} = g_i^{-1} \tilde{h}_{ij} g_j$, where g_i are unit quaternions. Hence $\tilde{\mathcal{E}}_{ij} = g_i^{-1} \mathcal{E}_{ij} g_j$. If we now look at an eigenfunction ϕ of the intrinsic Dirac operator on $\mathcal{X}$, it will satisfy

$$(D\phi)_i = \frac{1}{2}\sum_j \mathcal{E}_{ij}\phi_j = \lambda\phi_i.$$

and thus

$$\frac{1}{2}\sum_j g_i^{-1}\mathcal{E}_{ij}g_j g_j^{-1}\phi_j = \lambda g_i^{-1}\phi_i.$$

Plugging in the previous equation we get

$$\frac{1}{2}\sum_j \tilde{\mathcal{E}}_{ij}\tilde{\phi}_j = \lambda\tilde{\phi}_i$$

for $\tilde{\phi}_i = g_i^{-1}\phi_i$. Therefore λ and $\tilde{\phi}$ are the eigenvalue and eigenfunction of the intrinsic Dirac operator on $\tilde{\mathcal{X}}$.

Note that one can always right multiply ϕ with a constant quaternion q such that ϕq is again an eigenfunction with the same eigenvalue. This means that the eigenvalues of the operators on $\mathcal{X}$ and $\tilde{\mathcal{X}}$ correspond, and their eigenfunctions are of the form ϕ_i and $g_i^{-1}\phi_i q$ respectively. As a result, the norm of the intrinsic Dirac eigenfunctions is invariant to isometries, i.e. $|\phi_i| = |g_i^{-1}\phi_i q|$, since g_i and q have unit length. Moreover, the spin transformation of these two isometric surfaces according to those eigenfunctions (the Dirac immersions) are:

$$\begin{aligned}\mathcal{E}_{ij} &\mapsto \bar{\phi}_i\cdot\mathcal{E}_{ij}\cdot\phi_j\\ \tilde{\mathcal{E}}_{ij} &\mapsto \overline{g_i^{-1}\phi_i q}\cdot g_i^{-1}\mathcal{E}_{ij}g_j\cdot g_j^{-1}\phi_j q = \bar{q}\bar{\phi}_i\cdot\mathcal{E}_{ij}\cdot\phi_j q\end{aligned}$$

which only differ by a rotation represented by the unit norm q, meaning that they are related by a rigid transformation.

We can similarly prove that the extrinsic Dirac operator is covariant under rigid transformations, by replacing all per-face g_i above with a constant unit quaternion $g\in\mathbb{H}$, the same for all faces.

Discussion on spinor covariance. A reasonable question might be why the eigenfunction is not invariant under isometric deformations but differs by the factor g_i^{-1}, given that the Dirac operator is intrinsic. In fact, the spinor eigenfunction, which is more like a vector field rather than a scalar field, will only be covariant rather than invariant under the coordinate transformation. For example, assume a vector field V with the expression $V = c_1e_1 + c_2e_2$ in a frame $\{e_1,e_2\}$. Then, in another frame (e_1',e_2') such that $(e_1',e_2') = (e_1,e_2)\cdot G$, the expression should change accordingly by $(c_1',c_2')^T = G\cdot(c_1,c_2)^T$. Analogously, the quaternion-valued function ϕ is actually the expression of the spinor with respect to a frame which is the pullback of a parallel frame by the immersion $f: M\to\mathbb{R}^3$. If one uses another isometric immersion $df' = g^{-1}dfg$, one should expect the corresponding spinor transforms like $\phi\mapsto g^{-1}\phi$.

Proof of Theorem 5.1. The first eigenvalue for the spherical surface has the estimated bounds [Bär98]:

$$\frac{4\pi}{\text{Area}} \le \lambda_1^2 \le \frac{1}{\text{Area}}\int_M H^2 \tag{32}$$

Hence the immersion induced by the $D\phi = \lambda_1\phi$ has the mean curvature half-density

$$h = \lambda_1|df| \le \sqrt{\frac{1}{\text{Area}}\int_M H^2}|df|$$

By $W = \int h^2$ we have

$$W_1 \le \left(\frac{1}{\text{Area}}\int_M H^2\right)\int_M |df|^2 = \int_M H^2 = W$$

Proof of Theorem 5.2. Two nets $\mathcal{X}$, $\tilde{\mathcal{X}}$, which only differ by an Euclidean motion, are related by

$$\begin{aligned}\tilde{E}_{ij} &= g^{-1}\cdot E_{ij}\cdot g\\ \tilde{n}_i &= g^{-1}\cdot n_i\cdot g\end{aligned}$$

where g is constant and has unit length. By the same argument as in the proof of Theorem 4.3 above, any eigenfunction ϕ_i of the intrinsic or extrinsic Dirac operator on $\mathcal{X}$ is corresponding to the eigenfunction $g\phi$ on $\tilde{\mathcal{X}}$. Besides, any two eigenfunctions corresponding to the same eigenvalue might differ by a right multiplication of a unit quaternion $q\in\mathbb{H}$. Taking this into account, corresponding eigenfunctions of $\mathcal{X}$ and $\tilde{\mathcal{X}}$ will have the form ϕ and $g^{-1}\phi q$. Now let's take the canonical representation proposed in [LJC17, Section 4.3]:

$$\begin{aligned}\phi &\mapsto \phi\cdot\frac{(\sum_i c_i\phi_i)^{-1}}{|(\sum_i c_i\phi_i)^{-1}|}\\ g\phi q &\mapsto g\phi\cdot\frac{(\sum_i c_i\phi_i)^{-1}}{|(\sum_i c_i\phi_i)^{-1}|}g^{-1}\end{aligned}$$

where c_i are some fixed real numbers, particularly in [LJC17] they are set to be the areas. It is easy to see that these two eigenfunctions belong to the same conjugate class. Therefore we have the following two rigid-transform invariants:

- The rotation angle, or the normalized real part, $\cos\frac{\theta_i}{2}$, which is invariant under the conjugate class.
- The angle between the rotation axis and the face normal $\langle u_i,n_i\rangle$, because

$$\langle u_i,n_i\rangle = \langle gu_ig^{-1},gn_ig^{-1}\rangle$$